

Persistent Deformation in a Post-Collisional Stable Continental Region: Insights from 20 Years of cGPS in Romania

Alexandra Muntean^{1*}, Laura Petrescu^{1,2}, Boudewijn Ambrosius³, Felix Borleanu¹, Eduard Ilie Nastase¹, Ioan Munteanu^{4,5}

1. National Institute for Earth Physics, Magurele, 077125, Romania
2. Faculty of Physics, University of Bucharest, Magurele, 077125, Romania
3. Faculty of Aerospace Engineering, Delft University of Technology, Delft, 2629HS, The Netherlands
4. Faculty of Geology and Geophysics, University of Bucharest, Bucharest, 010041, Romania
5. Romanian Academy Institute for Geodynamics “Sabba Stefanescu”, Bucharest, 020032, Romania

Correspondence to: Alexandra Muntean (muntean@infp.ro), Laura Petrescu (laura.petrescu@infp.ro), Boudewijn Ambrosius (bacambrosius@gmail.com).

Abstract. The Carpathian Region, located at the edge of the East European Platform, presents a unique tectonic setting where major deformation associated with subduction and collision appears to have ceased around 8 million years ago. Yet vertical movements and present-day seismicity continued afterward, suggesting ongoing crustal deformation and challenging our understanding of intraplate earthquakes and the processes driving these phenomena in an area considered a stable continental interior. In this study, we analyze over two decades of continuous GPS (cGPS) data from 143 permanent stations to estimate both horizontal and vertical crustal motions, constructing the most accurate model of crustal deformation in the region to date. The estimated velocity field indicates a southward drift of the South Carpathians and Moesia relative to Eurasia, with velocities ranging from 0.5 to 2 mm/yr. We detect a more complex pattern of vertical uplift and subsidence in the foredeep, challenging a previously held view that this region is solely subsiding. This pattern may reflect localized uplift in response to processes such as the Vrancea Sslab break-off beneath the South-East Carpathians. Crustal scale active faults accommodate the observed differential motion, fragmenting the foreland. Furthermore, using a regularized horizontal velocity vector field, we estimate strain rate variations, maximum shear strain, and dilatation patterns across Romania, which closely align with observed crustal earthquake mechanisms. This agreement validates our results and indicates a significant influence of surface plate kinematics on the observed seismicity, in addition to the deep Vrancea Sslab dynamics. Our findings provide fundamental insights into the causes of crustal deformation at the transition between active collision zones and stable continental platforms, enhancing our understanding of intraplate seismicity in regions traditionally considered tectonically stable.

Keywords: deformation, GPS, crustal motion, geology, tectonics

1. Introduction

A key tectonic question lies in understanding the nature of active deformation and frequent seismicity in regions situated at the transition between active subduction/collision systems and more stable continental interiors. The Carpathian Region in Romania marks such a transition between the active Africa-Eurasia subduction system to the south and the stable continental core of Eurasia: the East European Platform (Fig. 1). Although this area is not considered a traditionally active plate boundary, with most geological evidence suggesting that major deformation

38 associated with the collision ceased around 8 million years ago (Mațenco and Bertotti, 2000), it continues to
39 experience frequent crustal and subcrustal seismicity. Active deformation and seismicity are observed along major
40 faults and geological contacts (e.g., swarms near Tg. Jiu and Galați, Craiu et al., 2017~~23~~; Radulian et al., 2023;
41 Borleanu et al., 2024). Notably, the Vrancea Sslab, a relic lithospheric plate sinking, retreating and stretching
42 beneath the East Carpathians Bend Zone, may still be coupled with the overlying crust, as suggested by the
43 thermochronological studies, which showed a significant amount of uplift, post 8 Ma, especially along the Western
44 flank of Focsani Basin (Necea et al., 2005, 2013, 2021, ~~Fig. S1 in the Supplementary Material~~). This coupling
45 could be driving long-term surface deformation (Ismail-Zadeh, 2012; Petrescu et al., 2021), contributing to
46 ongoing seismicity (Radulian et al., 2019, 2023; Petrescu et al., 2025) and exhibiting the largest present-day strain
47 concentration in continental Europe (Wenzel et al., 1999).

48 Measuring crustal motion is crucial for understanding ongoing deformation processes and seismic hazards in such
49 a tectonically complex region. In this study, we estimate both horizontal and vertical motions using Global
50 Positioning System (GPS) data from permanent stations that operated in Romania in the past 20 years. These
51 measurements provide key information about how the region is deforming and how this relates to the observed
52 seismicity. The data also shed light on the connection between surface deformation and subsurface dynamics,
53 including the potential role of the sinking slab in driving seismic activity. Furthermore, the GPS data allows us to
54 assess whether deformation is concentrated along major fault zones or more broadly distributed across the crust,
55 offering a clearer picture of how past tectonic events continue to shape the region's seismic behavior.

56 The first vertical velocity maps of Romania, based on repeated leveling data from first- and second-order national
57 network lines, were published by Cornea et al. 1978, 1978~~9a~~ 1979b. Following the major earthquake of March 4,
58 1977 (M7.2), high-accuracy leveling measurements allowed for the development of a more refined vertical
59 velocity map (Popescu and Dragoescu, 1987). Subsequent research extended these efforts to the broader Carpatho-
60 Balkan region (Joo et al., 1987). Dinter and Schmitt (2001), after two years of GPS monitoring in Romania, found
61 no significant deformation but recommended expanding the network and conducting repeated measurements at
62 two-year intervals to capture crustal dynamics better. Van der Hoeven et al. (2005) later published results from
63 annual GPS campaigns conducted between 1997 and 2004. However, velocity solutions derived from temporary
64 GPS deployments were subject to influences such as equipment changes, monument removals, and antenna setup
65 inconsistencies, as well as local effects like sediment compaction and site instability. Compared to the high
66 precision of modern continuous GPS (cGPS) solutions, the historical campaign data exhibit 3 to 4 times higher
67 uncertainty (van der Hoeven et al., 2005). These limitations highlight the need for continuous GPS measurements
68 to better resolve crustal and mantle dynamics in geologically active regions.

69 **2. Tectonic setting**

70 The tectonic evolution of the Romanian region is essential for understanding present-day deformation and seismic
71 activity. The Carpathian Mountains dominate the topography, but significant faulting and seismicity are pervasive
72 in the South and Southeast Carpathians and the surrounding foreland (Petrescu et al., 2021), underlain by the
73 Moesian Platform (MP), a thick lithospheric block with Precambrian-aged basement, shaped by multiple tectonic
74 phases throughout the Paleozoic and Mesozoic times (Fig. 1). **The Moesian Platform (MP) is bounded by the**

75 Carpathians to the north and the Balkans to the south. It is largely covered by Neogene sediments and extends
76 eastward to the Black Sea, where its uplifted basement is exposed in the Dobrogea region. The platform is
77 transected by several crustal-scale faults, such as the Intra-Moesian Fault (IMF) and the Capidava-Ovidiu Fault
78 (COF) (Fig. 1).

79 To the northeast, the MP transitions into the East European Platform (EEP), a thick and geologically stable
80 continental core that forms part of the Eurasian Plate. The boundary between the two is marked by ~~a series of~~
81 ~~crustal-scale faults and~~ the North Dobrogea Orogen (NDO) (Hippolyte, 2002), a remnant of the Hercynian
82 Orogeny (Seghedi et al., 1999), located between the Peceneaga-Camena Fault (PCF) and Sfântul Gheorghe Fault
83 (SFG, Fig. 1). Part of this now partially eroded orogen is buried beneath Neogene foredeep sediments from the
84 younger Carpathian collision, while to the east, it has undergone uplift.

85 Over the past 20 million years, the Adria Plate, a promontory of the African or Nubian plate, has continuously
86 pushed other oceanic plates and microplates north and east, leading to their collision with the stable Eurasian
87 terranes and driving the Alpine-Carpathian orogeny (Balla, 1986; Barrier et al. 2018), essentially shaping the
88 present-day European continent (Schmidt et al., 2020). In Romania, these microplates have been obliquely thrust
89 over the MP, forming the South Carpathians, and collided with the passive margin of the East European Platform,
90 creating a series of thrust faults and thin-skinned sedimentary nappes that make up the East Carpathians
91 (Sandulescu, 1984; Mañenco and Bertotti, 2000; Csontos and Vörös, 2004).

92 Beneath the Southeast Carpathians, where multiple tectonic units interact, the notorious Vrancea Sslab, a
93 lithospheric block that is plunging almost vertically into the mantle, stretching and generating frequent high-
94 magnitude destructive earthquakes in Romania, both at intermediate depths and in the overlying crust (Radulian
95 et al., 2019; Petrescu et al., 2021; Enescu et al., 2023). Observing the crustal motions above this sinking slab
96 provides a unique opportunity to gain fundamental insights into crustal deformation in a triple-junction tectonic
97 setting (Besutiu et al., 2019). Major collisional related shortening deformation in the Carpathians is thought to
98 have ended around 8-11 Ma, based on the cessation of late Miocene thrusting (Mañenco et al., 2007 and references
99 therein), while fission-track analysis suggests the onset of exhumation (or uplift) at 4 Ma in the SE Carpathians
100 and 12 Ma in the East and South Carpathians (Sanders et al., 1999; Cloetingh et al., 2006). Present-day GPS
101 measurements provide key insights into how these long-term geological processes continue to shape ongoing
102 crustal motion and deformation, particularly in the Vrancea Zone (Fig. 1), where active subduction and slab-
103 related dynamics are still influencing surface motion. The crustal deformations observed today are also influenced
104 by the relative motion of surrounding crustal blocks, complicating the understanding of the region's complex and
105 dynamic geological behavior.

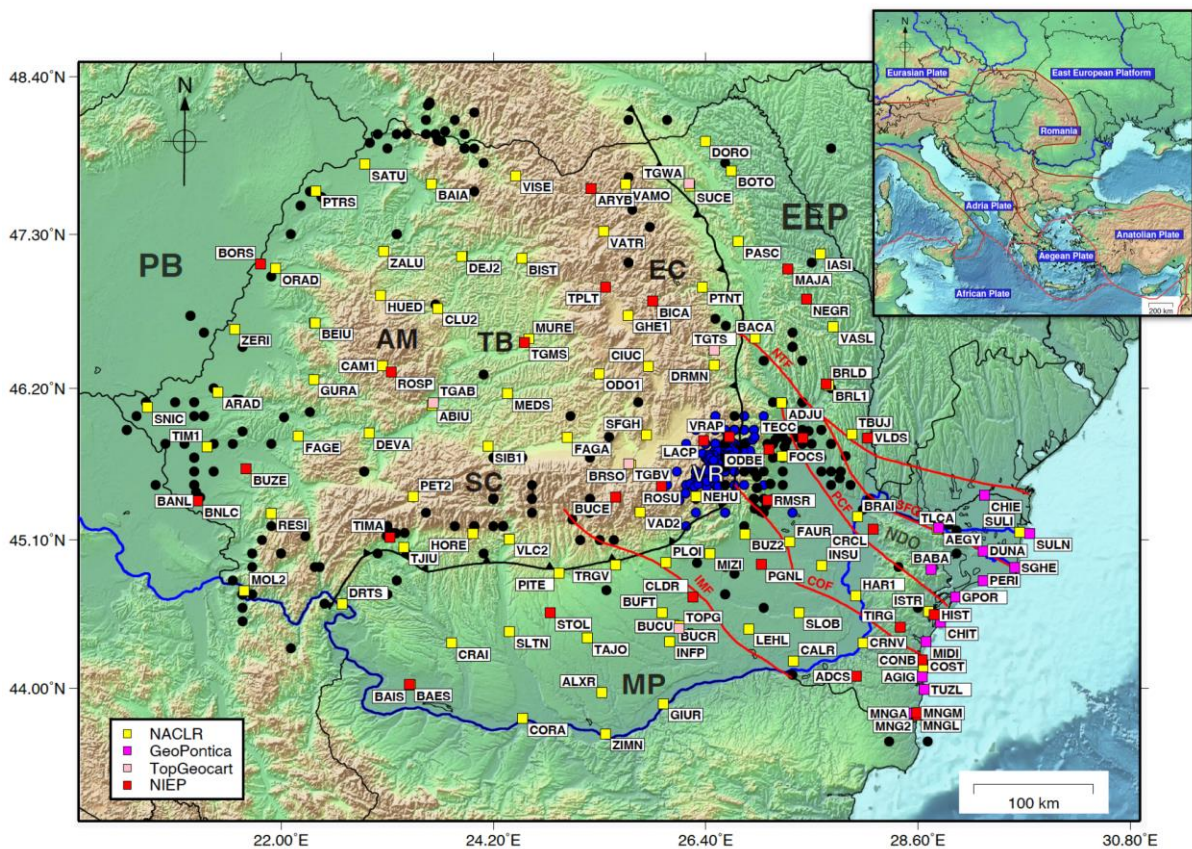
106 3. Continuous GPS (cGPS) Networks in Romania

107 We analyzed data from cGPS stations across Romania ~~and surrounding regions~~, which are part of ~~several~~ **four**
108 different networks (Fig. 1). The primary network, supported by the National Institute for Earth Physics (NIEP),
109 was first developed in 2001. Initially, the network consisted of seven stations, equipped with Leica CRS1000
110 receivers and LEIAT504 choke-ring antenna protected by a dome. These stations were placed in remote areas
111 and were designed to operate with minimal maintenance, relying on power converters and batteries. Over time,

112 the network has grown , and today it includes 33 stations, with five of the original stations still in use. The
 113 newer stations are equipped with Leica GRX1200, LEIAR GR30, and GR50 receivers. Most of the antennas are
 114 Leica (LEIAT504, LEIAR10, LEIAR20) and are placed on concrete pillars. Only one is mounted on a polar mast
 115 (MNG2). The stations transmit real-time data via the internet, and NIEP is responsible for the equipment,
 116 installation, ongoing maintenance, and data analysis.

117 We also used GPS data from the GeoPontica network, developed by the National Research and Development
 118 Institute for Marine Geology and Geoecology (GeoEcoMar), the National Center for Monitoring and Alarm to
 119 Natural Marine Hazards – Euxinus, covering the period from 2013 to the present. This network includes 13
 120 stations, the antennas are mounted on a deep-drilled braced monument. In addition, we included data from the
 121 ROMPOS (NACLR) network, managed by the National Agency for Cadastral and Land Registration, which
 122 consists of 86 reference stations across Romania. (Fig. 1). We were also granted access to data from the private
 123 TopGeocart network, which includes 8 stations. Most of these GPS antennas are mounted on building rooftops or
 124 fixed to the structures housing the receivers.

125 In total, this selection resulted in 143 available stations. The data are stored in a repository, organized by network,
 126 year and Julian day, in the Receiver Independent Exchange (RINEX) version 2 and 3 format, sampled at 30s
 127 intervals. For this study, we only selected stations that are (still) operational after January 01, 2024. This reduced
 128 the selection to 130 stations. Their locations and station acronyms are presented in Figure 1.



129
 130 **Figure 1: Map of Romania showing the distribution of the available GPS stations used in this study (coloured**
 131 **squares), tectonic regions, and major faults and tectonic boundaries (thick black lines), and epicentres of earthquakes**
 132 **with Mw > 3.5 recorded in the Romanian earthquakes catalog (Romplus, Popa et al., 2022). Earthquakes are color-**
 133 **coded by depth: black for crustal events (H < 60 km), blue for intermediate-depth events. The major faults are plotted**

134 as solid red lines and identified with their acronyms in a blue box: IMF - Intra-Moesian Fault, COF - Capidava Ovidiu
135 Fault, PCF - Peceneaga Camena Fault, NTF - New Trotuș-Fault, and SFG - Sfântu Gheorghe Fault. The old trust
136 fault is represented by a solid, black, toothed line. The major tectonic units are in bold white characters: AM - Apuseni
137 Mountains, SC - South Carpathians, EC - East Carpathians, VR - Vrancea, NDO - North Dobrogea Orogen, PB -
138 Pannonian Basin, TB - Transylvanian Basin, EEP - East European Platform, and MP - Moesian Platform. Further
139 acronyms in the color legend box include: NACLRL - National Agency for Cadastre and Land Registration, GeoPontica
140 - National Research-Development Institute for Marine Geology and Geoecology GNSS network, TopGeocart is a
141 private company, operating its own GNSS network, NIEP- National Institute for Earth Physics. The inset shows the
142 regional tectonic setting, with plate boundaries indicated in red.

143 4. GPS data processing

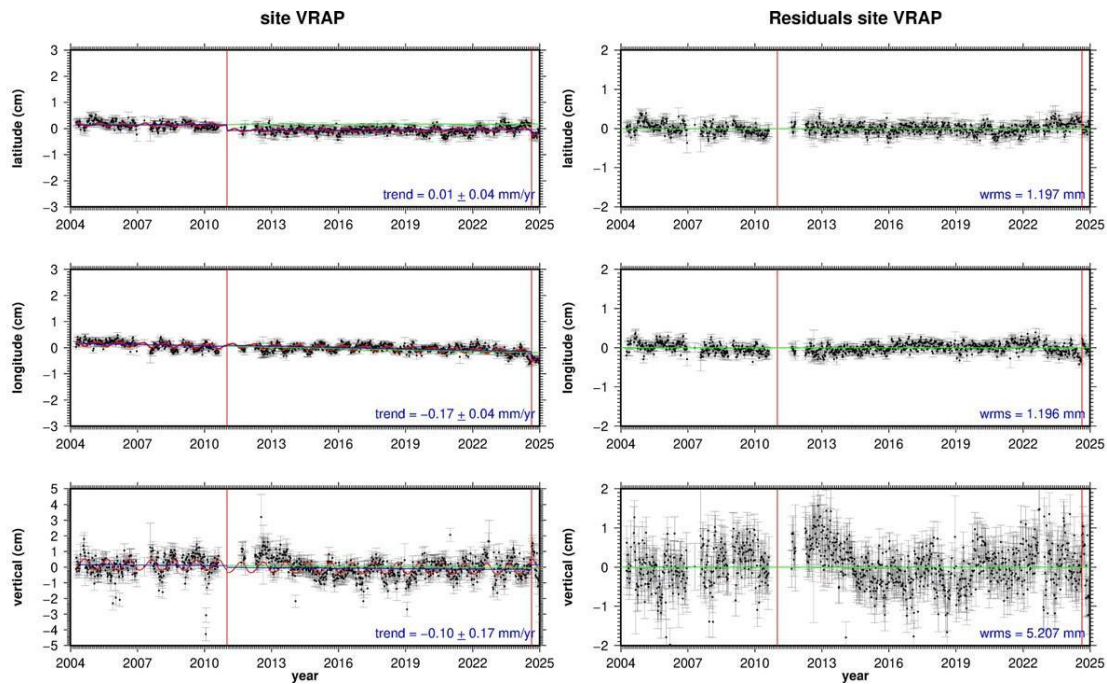
144 For the data processing, we use the GipsyX software (Bertiger et al., 2020), developed at NASA's Jet Propulsion
145 Laboratory (JPL), Pasadena, USA. It features Precise Point Positioning (PPP), which enables (daily) geodetic
146 position determination of a single GPS station. Accuracy can vary depending on the quality of the GPS receiver,
147 the antenna, and local conditions (e.g., multipath). Weekly updated data files, provided by JPL, contain precise
148 GPS satellite orbits, Earth Rotation Parameters (ERP), satellite clock corrections, spacecraft altitude information,
149 and so-called wide lane phase biases to enable signal ambiguity resolution. In addition, we apply ocean loading
150 corrections for each station, obtained from the Onsala Space Observatory, Chalmers University of Technology
151 (Bos and Scherneck, 2011). To model the wet tropospheric signal delays, we use data from VMF (Vienna Mapping
152 Functions) (re3data.org:VMF Data Server).

153 All available RINEX data files are stored in a database, organized by network, year, and Julian day. All eGPS
154 data used in this study are in the Receiver Independent Exchange (RINEX) version 2 and 3 format. To homogenize
155 the processing, we only use GPS data, sampled at a period of 30s. The processing with GipsyX resulted in a
156 similar database with daily solutions for each station (Fig. 2) in the ITRF14 reference frame (Altamimi et al.,
157 2016).

158 To reduce the noise level, we combine the daily GPS positioning solutions into weekly solutions. Using our
159 software, we convert these solutions to the Eurasian tectonic reference plate using the most recently published
160 rotation pole solution of that plate. This results in a time series of latitude, longitude, and height components.
161 From these time series, we calculate a linear trend (velocity) and yearly and half yearly seasonal signals (Fig. 2).

162 To account for antenna changes that were not documented in the metadata, we also estimate position jumps at the
163 times where we notice these changes (Fig. 2).

164 Processing the recordings from the 130 selected stations with this software resulted in a repository with daily
165 solutions for each station. Subsequently, to reduce noise, we combined the daily solutions into weekly ones. Then,
166 we converted the reference plate of these solutions to the Eurasian tectonic reference plate using the ITRF14
167 rotation parameters of that plate (Altamimi et al., 2017). From this data, we created a time series for each station.
168 Next, we estimated a linear trend (velocity) and yearly and half-yearly seasonal signals. In addition, for
169 undocumented changes, the estimation model also includes position jumps at times identified from an inspection
170 of the raw time series. All recent time series are affected by a reference frame change on August 19, 2024, by
171 JPL. These are now also modeled as position jumps. An example of the results is presented in Figure 2 for the
172 long-lived station VRAP. Apparently, this station was re-equipped in 2011, and from the vertical residuals, it
173 seems that it took a few years to settle down on its original monument.



174
175
176
177
178
179

Figure 2: Time series of the VRAP station. The left panel shows the raw series with the modeled functions. The red curve represents the estimated yearly and half-yearly functions, and blue lines indicates the estimated linear trend, and in the left panel the green curve correspond to the predicted values following line represents the estimated velocity before the first jump. The vertical red lines represent position jumps. The right panel shows the residuals after subtracting the modeled functions, including the estimated position jumps.

180 4.1 Horizontal time series data selection and quality control

181 Analysis of the 4 permanent Romanian networks resulted in 130 time series solutions for sites (still) operational
182 after January 01, 2024. The length of the time series varies from 0.6 to 22.4 years. Then we apply a model to these
183 time series consisting of a linear term (the velocity), yearly and half yearly terms, and position jumps for
184 undocumented antenna changes. Next, we apply a general editing criterion to only select solutions with an
185 accuracy (sigma) of 0.2 mm/yr.

186 In this step, finally, to ensure the best possible quality of the data time series solutions, we selected results stations
187 with uncertainties (sigmas) less than 0.2 mm/yr and velocity vectors smaller than 2 mm/yr. We consider that these
188 criteria guarantee a reliable selection of credible solutions. However, a small number of these sites still exhibit
189 anomalous velocities. These are likely caused by local effects such as landslides, station instability, local
190 geological conditions, subsurface compaction, undocumented antenna changes, and multipath interference. The
191 main reason is that most GPS antennas are mounted on buildings and unstable steel rods. Therefore, we added
192 another editing step, described in the following paragraph. In our analysis, we try to model them as position jumps.
193 The dates of these “unknown” jumps were established using a manual process by examining the “raw” time series
194 plots for each station.

195 This process automatically eliminates the shorter lived time series, reducing the number of accepted solutions to
196 99, with the shortest series spanning extending 4.4 more than four years. This means that all 99 accepted solutions
197 satisfy the criterion established by Blewitt et al. (2001), who claim that the series should be longer than two and
198 a half 2.23 years for a reliable estimate of the seasonal terms, which is vital for the reliability of the velocity
199 estimate.

200 The results for the 99 accepted sites are summarized in Table S1. Examples of a well behaved site, BICA and
201 ROSP, and problematic sites such as BRAI and STOL are given in Supplementary Material (Fig. S2 and S3). The
202 latitude component of STOL also demonstrates that there can be significant seasonal variations, which can occur
203 for any site and any component for unknown reasons. Part of the selection was a manual process, based on
204 examining the time series plots for each site.

205 The accuracies (σ) at the 95% confidence level were estimated using the weighted root mean square (WRMS) of
206 the fit according to the formula:

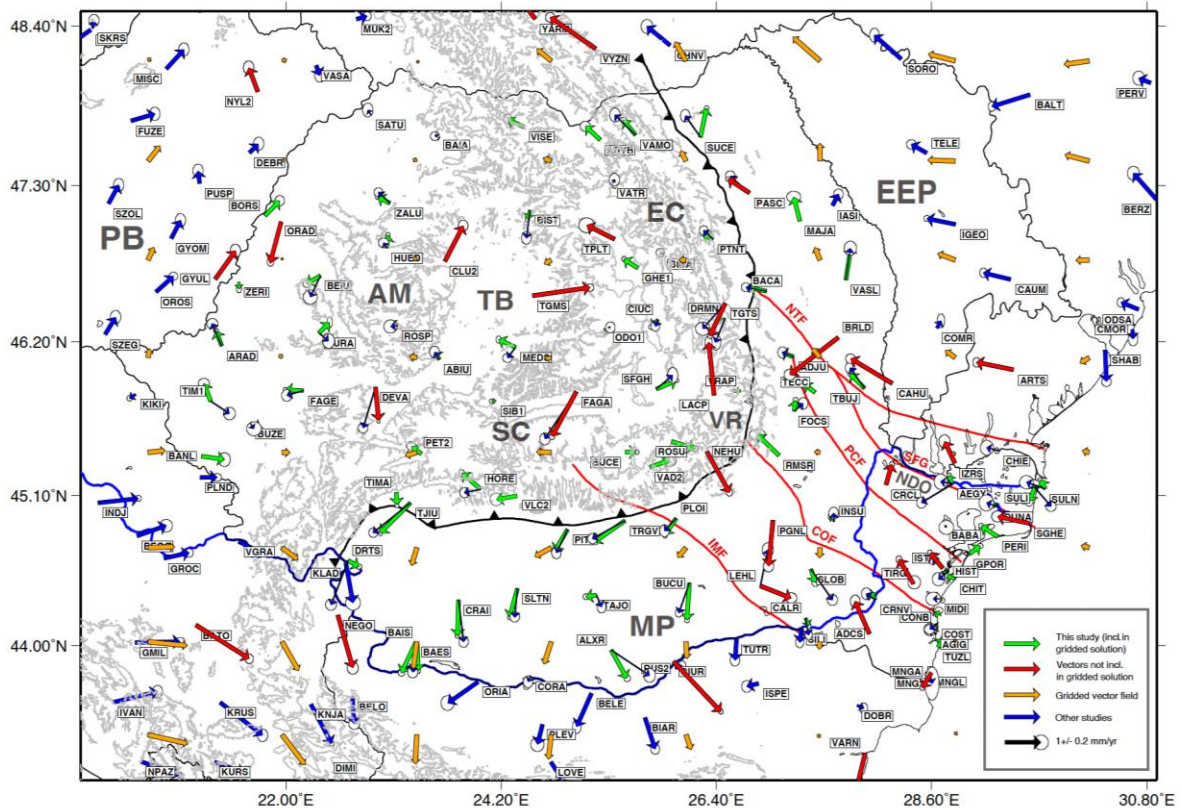
207
$$\sigma = \frac{2 \cdot WRMS}{2.4 \cdot T_{span}}$$

208 where T_{span} is the length of the time series in years. This approach provides robust and realistic estimates of
209 velocities and their uncertainties, and yields results comparable with those obtained using other commonly used
210 algorithms, such as HECTOR and MIDAS. For some stations, our uncertainties are smaller than literature values,
211 which is primarily due to the longer time series used in this study. We also compared our results with those of
212 Piña-Valdés (2022) for stations with common solutions and found an average difference of less than 0.08 mm/yr.
213 This level of agreement demonstrates general consistency, although earlier processing campaigns did not benefit
214 from the reprocessing strategies and data quality controls applied here. The results for the 99 accepted sites are
215 summarized in Table S1 of the Supplementary Material.

216 ~~4.2 Estimating~~ **4.2 Creating a gridded, smoother horizontal velocity field**

217 To ~~derive~~ **create** a smooth, coherent representation of the computed time series solutions, we use a spatial gridding
218 approach: we set up an 8 x 8 grid of latitude and longitude nodes with each node linked to a square search box.
219 The size of these boxes ~~is based~~ **depends** on the distance (in km) between ~~neighbouring~~ **nearby** nodes, ~~making~~
220 **sure ensuring** the north-south and east-west dimensions are equal. ~~in kilometers. Inside each search box,~~ **W**
221 **we** calculate the median of the absolute velocity vectors of the sites ~~contained~~ **inside each search** the box. In the ~~final~~
222 **next** step, we eliminate outliers with a velocity larger than ~~2~~ **two** times the median. ~~Then~~ **In the final step,** we
223 calculate the average of the EW and NS velocity components of the remaining solutions. ~~In~~ **During** this process,
224 22 of the 99 solutions are excluded as outliers. The final result is a gridded dataset ~~showing velocities for each~~
225 **node, with some nodes left blank where no stations are available in the search area (Fig. 3).** ~~of 47 nodes showing~~
226 **the velocities for each node. The other 17 nodes are not presented since there were no Romanian cGPS stations**
227 **available in the search area (see Table S2, SM).**

228 When we include the literature (Pina-Valdes et al., 2022; Serpelloni et al., 2022), solutions for the countries
229 neighbouring Romania, the number of solutions increases to 160. After applying the aforementioned editing step,
230 this number decreases to 133. These solutions are based on a collection of shorter time series from before 2021.
231 Nevertheless, they provide valuable additional information.



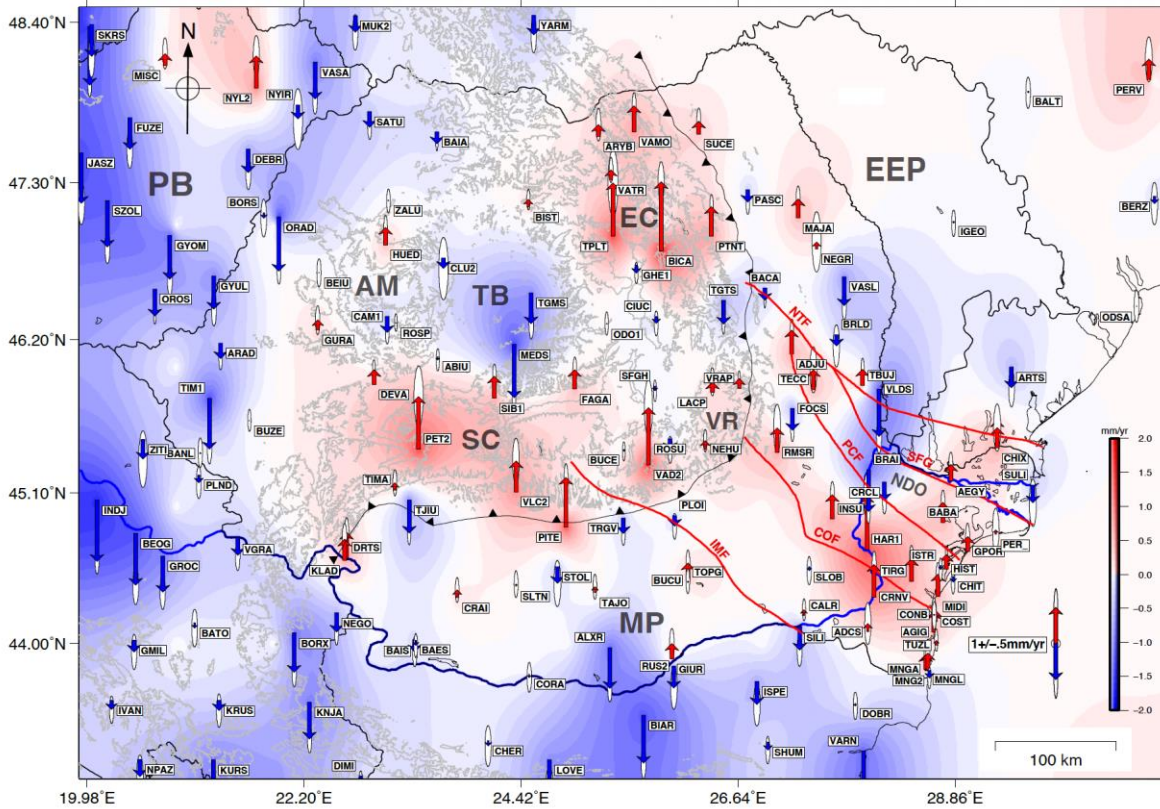
232
233
234
235
236
237
238

Figure 3: GPS-estimated derived horizontal velocity vectors with respect to Eurasia Plate derived from the the ITRF-2014 Eurasian plate according to Altamimi et al. (2017). Green vectors represent our results, blue vectors were taken from Pina Valdes et al. (2022). The red vectors were excluded while creating the interpolated velocity field on a regular (8 x 8) grid, represented as orange vectors. The error ellipses are 95% confidence level. Red arrows represent the interpolated vector field on a regular grid. Faults and acronyms are as in Figure 1.

239 4.3 Vertical data selection

240 For the vertical component, we apply a different approach. This component is hardly affected by horizontal station
241 instabilities, but mostly by undocumented antenna changes. We tackle this problem by estimating vertical position
242 jumps at the dates when we see them appearing in the time series. Furthermore, we only select solutions with an
243 absolute velocity of < 2 mm/yr and an accuracy of < 1.0 mm/yr, which we consider to be credible solutions. Some
244 sites show larger subsidence, but these are mostly located in coastal areas, on slow landslides, and compacting
245 sedimentary areas. As a result, from the 130 available solutions of the four Romanian permanent networks, 95
246 106 solutions were accepted (Fig. 4). The results are presented in Figure 4 and Table S3 (SM). We also compared
247 our solutions with those of Piña-Valdés (2022), and found an average difference of less than 0.03 mm/yr.

248 When we include the literature solutions, the pattern does not change much. It mostly adds subsidence sites in the
249 area west and south-west of Romania (Table S2). The total number of accepted vertical sites increased to 145 156.



250
251
252
253
254
255

Figure 4: eGPS-estimated **derived** vertical velocity vectors, with respect to a background zero velocity field. The major faults are depicted by thick red lines. Bold red acronyms for the tectonic units are as in Fig. 1. A **red** vectors indicates an upward motion **uplift**, while a blue vectors indicates a downward motion **subsidence**. The background is a **gridded interpolation field**. The error ellipses are 95% confidence level. The abbreviations **Faults and acronyms** are as in **Figure 1**.

256 **4.4 Strain rate estimation**

257 To better understand deformation and seismic hazard in this complex tectonic region, we further estimate strain rate from the interpolated horizontal vector field of GPS velocities (Fig. 3). We use the open-source software
258 STRAINTOOL, which employs the VISR (Velocity Interpolation for Strain Rate) algorithm developed by Shen
259 et al. (2015). This algorithm interpolates ~~geodetic velocity data~~ **our gridded solution** to derive horizontal strain rates across the region, using a weighted least squares approach on a **more dense** regular grid. At each ~~site~~ **grid**
261 **point**, the horizontal velocity field is approximated by a bilinear function and a Gaussian function based on the
262 distance between the interpolation ~~site~~ **grid** point and the other grid points is used for distance-weighting. This
263 algorithm allows us to obtain the spatial variation of strain rate, including the maximum shear strain rate (which
264 indicates how much the crust is laterally distorted), and the dilatational strain rate (which reflects areas of
265 extension or compression). These parameters are crucial for understanding the tectonic regime, whether a region
266 is being compressed, extended, or sheared, and how this deformation relates to observed earthquake focal
267 mechanisms.
268

269
270
271

272 5. Results

273 5.1 The horizontal velocity field

274 Many horizontal velocity measurements indicate a predominantly southward movement in the MP, with variations
275 spanning approximately ± 20 degrees toward the southeast and southwest (Fig. 3). The IMF appears to mark a
276 slight orientation change from S-SE to S-SW oriented motion vectors. This shift is also reflected in the South
277 Carpathians, which are obliquely thrust over the MP, defined by strong and sometimes sharp lateral variation in
278 rheology across the major faults like IMF or COF, which imposed the formation of tear-faults and oblique ramps
279 into the Carpathian Orogen (Fig. 3). Hence, the magnitude and direction of motion vary significantly across the
280 IMF and COF or other major faults in the MP and foreland units in general, like PCF and TF, that are defining
281 crustal blocks with different rheologies, thermal history, and response under the orogenic loading. In contrast,
282 vectors in the East European Platform (EEP) ~~appear to~~ show a slight northwestward motion relative to the Eurasian
283 plate. This shift occurs across the PCF and TF, which define the boundaries of the North-Dobrogea Orogen (Fig.
284 3 ~~and S1~~), a transitional zone between the EEP margin and the MP. As a result, the EEP undergoes a subtle yet
285 persistent movement relative to Eurasia, diverging from the southward-moving MP through a series of crustal-
286 scale faults that accommodate lateral displacement.

287 The Transylvanian Basin (TB) and the East Carpathians, on the other hand, show minimal horizontal motion. GPS
288 stations in these areas indicate limited deformation, with inconsistent directional patterns and low overall
289 coherence in movement. Small horizontal motions are observed in the Pannonian Basin (PB) with an NNE
290 direction, which gets reoriented close to the Apuseni Mountains in different directions (see Figs. 1 and 3).

291 Overall, the foreland region, particularly the MP, seems to be drifting southward, while the other areas remain
292 relatively stable, indicating that the foreland is more dynamically active in comparison to the surrounding regions.

293 5.2 The vertical velocity field

294 The Carpathians predominantly experience significant uplift (Fig. 4), ~~with the strongest upward velocity vectors~~
295 ~~concentrated in localized areas of~~ **concentrated in** the East Carpathians (e.g., BICA, TPLT, ~~see Fig. 4~~) **and the**
296 **South Carpathians (e.g., VAD2, and PITE)**. While some scattered stations (ROSU, TGTS) indicate subsidence,
297 the overall trend suggests uplift rates ranging between 0.5 and 2 mm/yr. ~~The subsiding stations are located in the~~
298 ~~East Carpathians Bend Zone and Quaternary depressions and in the Transylvanian Basin situated in the core of~~
299 ~~the Romanian Carpathians (Fig. 4).~~ **The Vrancea Bend Zone is an interesting exception because it only shows a**
300 **minor uplift (e.g., LACP and VRAP).**

301 The foreland exhibits an intricate interplay of uplift and subsidence. ~~a complex pattern of vertical motions.~~ The
302 Moesian Platform (MP), **which occupies the area bounded by the Carpathians, the Balkans and the Black Sea,**
303 **shows a north-south dichotomy in vertical motion.** ~~displays an intricate interplay of uplift and subsidence (Fig.~~
304 ~~4).~~ In its southern part, **across the E-W trending Danube river and towards the Balkans,** the crust is predominantly
305 subsiding, **while Northward and northeastward** toward the Carpathians, ~~and the Capidava-Ovidiu Fault,~~ the trend
306 gradually transitions to uplift. ~~Northeast of the COF, several stations record uplift near the foredeep basin. Along~~
307 ~~the boundary with the EEP and the southeastern Carpathians, alternating zones of uplift and subsidence define a~~
308 ~~transitional belt. This spatial variation produces a distinctive pattern: subsidence along the PCF contrasts with~~

309 ~~uplift near the TF.~~ The most pronounced uplift occurs in Dobrogea, the exposed basement of the Moesian Platform
310 near the Black Sea, where all geodetic stations record consistent uplift along the coast and the Danube. Notably,
311 the Danube changes its course northward across this transition zone.

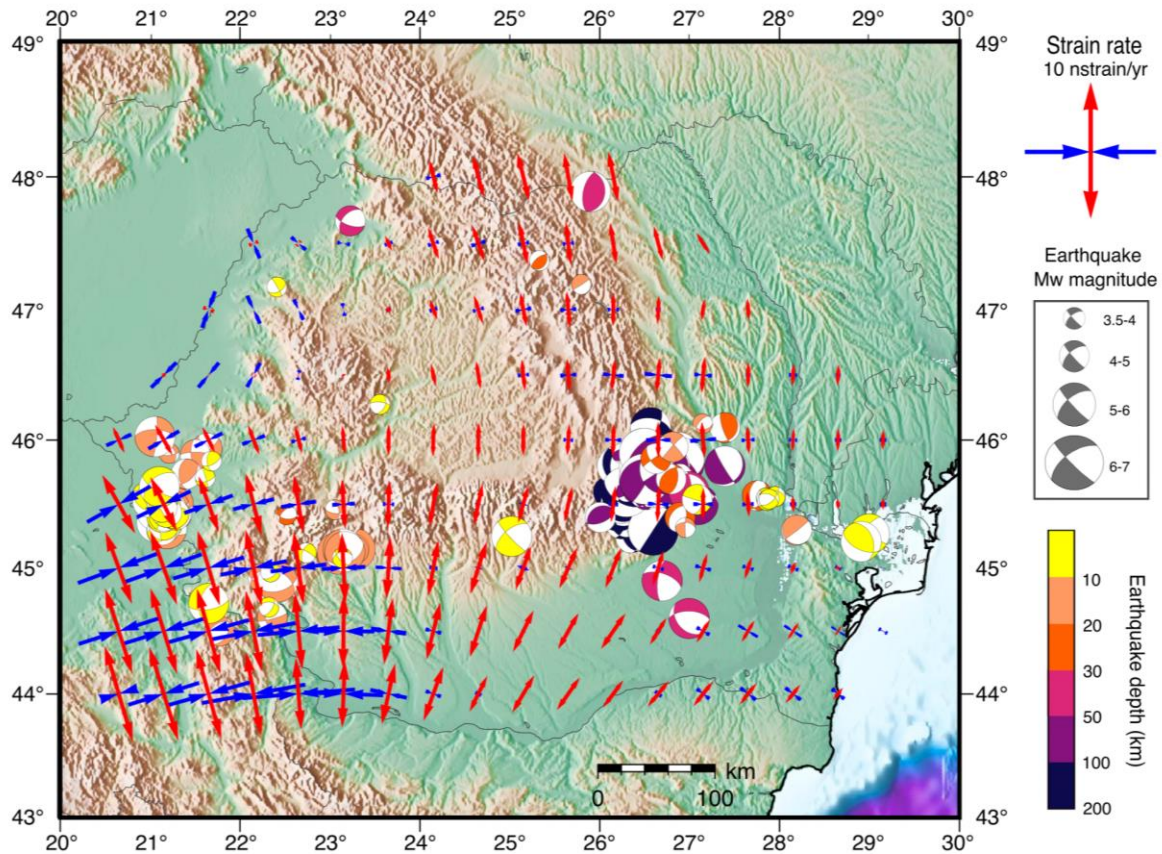
312 The East European Platform (EEP), forming the eastern foreland of the Carpathians, exhibits only minor vertical
313 movements. Several stations in its northern part record slight uplift, which transitions southward into subsidence
314 toward the Trotuș Fault. This subsiding trend extends farther south into parts of the North Dobrogea Orogen
315 (NDO), continuing across the SFG and the PCF, which delineates the boundary with the Moesian Platform (MP).
316 On the opposite side, the MP is undergoing uplift, reflecting strong differential crustal deformation along these
317 seismically active fault networks.

318 ~~Toward the Black Sea, vertical motion vectors suggest that the MP is undergoing consistent uplift in the coastal~~
319 ~~region (known as Dobrogea). The Dobrogea region, including MP and NDO (see Fig. 1 and Fig. S1 in the~~
320 ~~Supplementary Material), is experiencing uplift, defining a N-S trend different from the rest of the foreland~~
321 ~~system.~~

322 In the backarc region relative to the Carpathians, in the Transylvanian and Pannonian basins, estimated crustal
323 motions suggest subsidence relative to stable Eurasia. However, the Apuseni Mountains, a prominent highland
324 dividing the two subsiding basins, exhibit a cluster of stable and slightly uplifted motion vectors. **Plotted vectors**
325 **range between -2 and +2 mm/yr, with an uncertainty of 1.0 mm/yr (Table S3 of the SM). This is a general feature**
326 **for most stations in Europe.**

327 **5.3 GPS-estimated strain rates**

328 Figure 5 shows the estimated strain rate variation across Romania, from the regularized horizontal velocity vector
329 field, while Figs. 6a and b show the distribution of maximum shear strain rate and dilatation. The dilatation rate
330 quantifies the extent to which the Earth's crust is either expanding or contracting. It is derived by combining the
331 principal strain rates, with positive values indicating extension and negative values indicating contraction. High
332 positive dilatation values are indicative of regions experiencing extension, while negative values suggest
333 compression, as seen in processes like thrust faulting. On the other hand, the maximum shear strain rate measures
334 the degree of shear deformation within the crust, without affecting its overall volume. This is determined by
335 calculating the difference between the principal strain rates. Elevated shear strain rates are associated with regions
336 undergoing significant shear deformation, such as strike-slip fault zones, while lower values typically occur in
337 areas experiencing predominantly extensional or compressional deformation.



338

339 **Figure 5: Map showing the principal axes of strain rates determined from the smooth-regularized GPS**
 340 **horizontal velocity vector field from this study and mechanisms of earthquakes with $M_w > 3.5$ from the**
 341 **REFMC catalogue (Radulian et al., 2019). Major faults are depicted by thick black lines (see Figure 1).**

342 The distribution of strain rates is quite complex (Fig. 5 and Table S4, SM), which is expected given the region's
 343 complicated tectonic framework, with multiple blocks of diverse strengths converging to form a sinuous orogenic
 344 track. The highest strain rates were estimated in the southwest, at the border between Romania and Serbia. This
 345 region also experiences the highest shear strain rate (Fig. 6a).

346 Dilatation patterns estimated from the strain tensor show a transition from compression in the PB to extension in
 347 the intra-orogenic TB. The South Carpathians and the surrounding foreland regions, including the MP and the
 348 EEP, are predominantly characterized by extension (Fig. 6b). However, localized areas of compression are
 349 observed in the Eastern and South-East Carpathians, particularly in the Vrancea Zone.

350

351

352

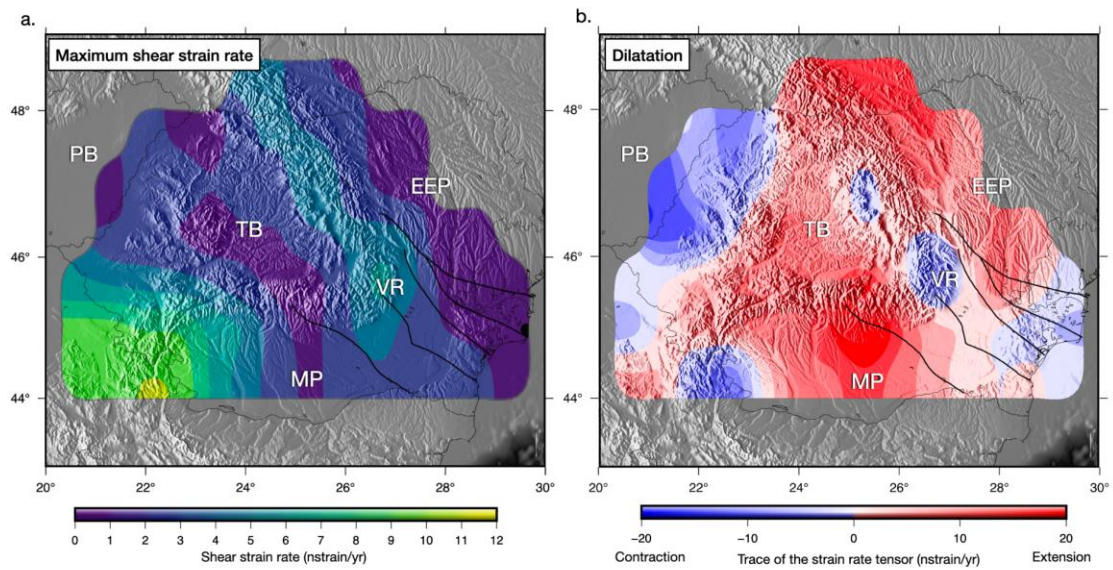
353

354

355

356

357



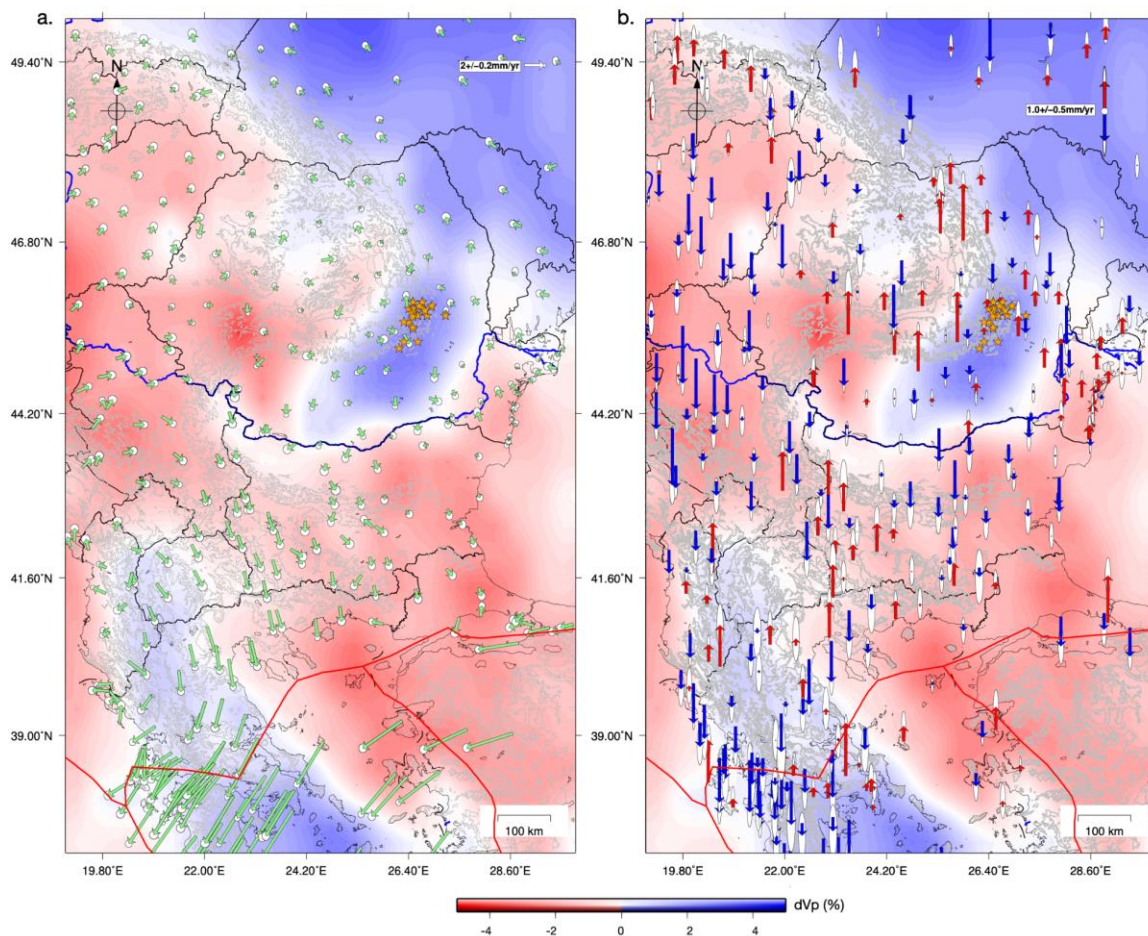
358 **Figure 6: Maps showing (a.) maximum shear strain rate and (b.) dilatational strain rate (both in**
 359 **nanostrain/year) derived from the average GPS velocity field the regularized GPS velocity field in Romania**
 360 **(Table S2, SM). The maximum shear strain rate illustrates the intensity and direction of lateral crustal**
 361 **deformation, while the dilatational strain rate is the trace of the strain rate tensor (volumetric rate of**
 362 **change) and indicates regions of extension (red-positive) and compression (blue-negative). Major faults are**
 363 **shown as thick black lines. (see Figure 1). Abbreviations are: PB – Pannonian Basin, TB – Transylvanian**
 364 **Basin, VR – Vrancea, MP – Moesian Platform, EEP – Eastern European Platform. Acronyms are described**
 365 **in the caption of Figure 1.**

366 6. Discussion

367 6.1 Regional tectonic context

368 To put our results in a broader context, we plot them in the context of against previous GPS-derived velocity
 369 vectors (Serpelloni et al., 2022; Piña-Valdés et al., 2022) in Fig. 7. While there is some overlap with the Romanian
 370 networks, the differences between datasets are minor. To reduce clutter in the figures and minimize the impact of
 371 large tectonic motions in the south, we excluded stations with an absolute horizontal velocity exceeding 7 mm/yr,
 372 as shown in Fig. 7a, horizontal, and 7b, vertical, with the UU-07 seismic tomography model of Amaru et al.

373 (2007), updated based on Wortel and Spakman (2000), at 200 km depth, serving as background



374

375 **Figure 7: Regional horizontal (a) and vertical crustal motions (b) from this study, Serpelloni et al. (2022), and Piña-**
376 **Valdés et al. (2022). The horizontal vector field was scaled for visibility. The background colours show Vp seismic**
377 **velocity anomalies at 200 km depth from the UU-P07 seismic model of Amaru et al. (2007). Red lines mark the active**
378 **plate boundaries between Eurasia, Anatolia, and Aegean plates in the south. Orange stars mark earthquakes Mw >**
379 **6 from the Vrancea Zone (Radulian et al., 2019).**

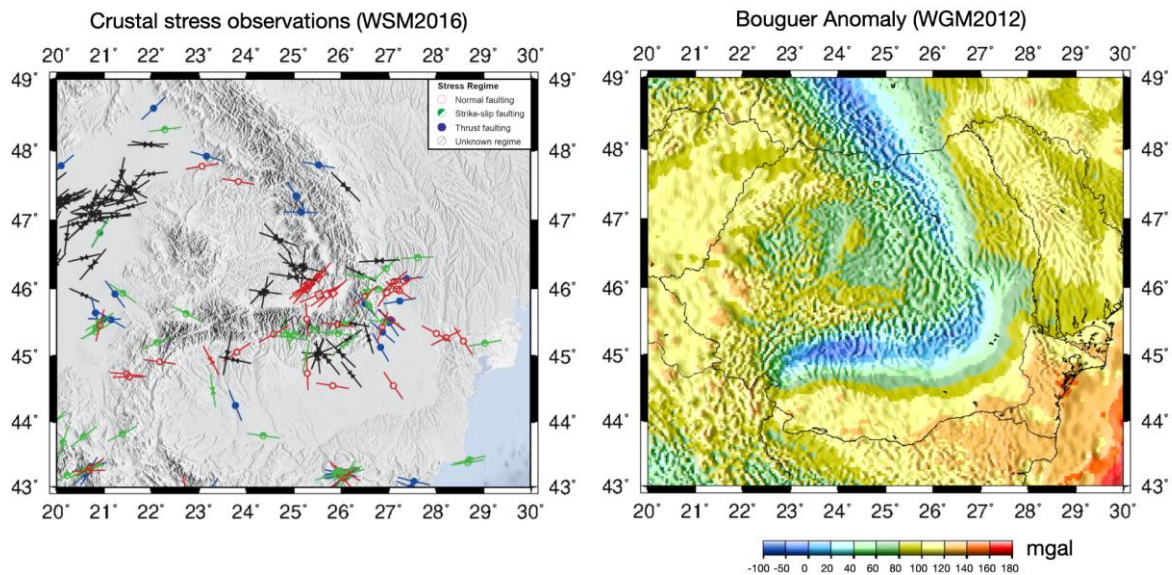
380 In the regional plate tectonic context, the observed velocity field highlights the complex interactions between
381 major tectonic plates and blocks that converged in this complex region. Seismic tomography shows the high
382 velocity thick cratonic lithosphere to the north-east, which is supposed to be tectonically stable, the Vrancea Slab
383 as an elongated high velocity block sinking beneath the Carpathians, and the Adria and the Hellenic slabs
384 subducting beneath the Balkan Peninsula (Fig. 7). To the south, crustal motion velocities increase significantly
385 (Fig. 7), reflecting the rapid motion of the Hellenic subduction system as the African Plate subducts beneath the
386 Eurasian Plate, driving southeastward deformation in Greece. Eastward, the Anatolian Plate is moving westward
387 due to tectonic escape caused by the northward collision of the Arabian Plate with Eurasia. This westward motion
388 is a dominant feature of the eastern Mediterranean and plays a key role in accommodating the overall regional
389 deformation.

390 To the west, the Pannonian Basin, a hyper-extended lithosphere back-arc basin, shows relatively low horizontal
391 deformation rates, suggesting it is currently tectonically stable, with mirror positive inversion of its eastern margin.
392 However, the influence of the Adriatic Plate, a promontory of the African Plate, is significant. The Adria Plate,
393 subducting eastwards (Fig. 7), exerts a northeastward push on the Carpathian-Pannonian system, contributing to

394 compressional forces and tectonic inversion along the basin (Bada et al, 2007). These larger-scale processes
 395 interact with the local tectonic architecture, such as the Vrancea Sslab and associated seismicity (orange stars in
 396 Fig. 7), resulting in a complex and heterogeneous deformation regime that bridges the stable cratonic lithosphere
 397 and the active subduction-driven tectonics to the south and south-west.

398 6.2 Correlation with fault systems and seismicity

399 Most seismically active crustal-scale faults and geological boundaries in Romania are located in the South and
 400 South-East Carpathians, as well as the foreland domains, which are crossed by several major faults (Fig. 1). While
 401 the Vrancea Sslab is well known for generating subcrustal earthquakes with a dominant reverse faulting
 402 mechanism in an overall compressive regime, the crust above exhibits much more diverse deformation (Fig. 5)
 403 and stress patterns (Fig. 8), likely driven by a combination of surface plate kinematics and Vrancea Sslab
 404 dynamics. Stress inversion of earthquake clusters in the crust (Petrescu et al., 2021) and geological indicators of
 405 stress from the World Stress Map (WSM2016, Heidbach et al., 2007) reveal a complex pattern of stress in the
 406 region (Fig. 8).



407 **Figure 8: Left: Crustal stress observations compiled from focal mechanisms, borehole breakouts, and other geological**
 408 **indicators, from the World Stress Map (Heidbach et al., 2016). Colours indicate the most likely stress regime. Right:**
 409 **Bouguer gravity anomalies from the World Gravity Map (WGM2012) maintained by the Bureau Gravimétrique**
 410 **International (Bonvalot et al., 2012).**

411 Although the GPS-derived strain rate field appears smooth at the regional scale, it consistently shows N-S
 412 extension throughout most of the study area and localized E-W compression in the southwestern corner (Fig. 6).
 413 This pattern reflects the long-wavelength deformation pattern resolved by the GPS velocity field, whereas the
 414 earthquake focal mechanisms capture the shorter-wavelength, fault-controlled deformation that accommodates
 415 this regional strain.

416 A localized cluster of thrust faulting stress regime indicators in the SE Carpathians broadly aligns with the negative
 417 dilatation rate derived from GPS vectors, suggesting localized compression at the bend zone (Fig. 6). This
 418 compressive region transitions into a mix of strike-slip and dominantly normal-faulting regimes (Fig. 8), aligning
 419 with our estimated dilatation rates that suggest an extensional regime throughout the foreland and the Carpathians
 420 (Fig. 6). This extension is supported by numerous normal fault earthquake swarms occurring near the SFG (Fig.

421 5 and Craiu et al., 2017). The South Carpathians have also recently experienced an intense seismic swarm of
422 normal-faulting earthquakes in the South Carpathians (Radulian et al., 2023; Borleanu et al., 2024).

423 At the same time, the variability of focal mechanisms, especially among smaller-magnitude events (Mw 3-4),
424 reflects the activation of secondary and oblique faults that accommodate local adjustments between the main
425 regional stress regimes. Even within the overall extensional setting, these structures produce local pockets of
426 compression or shear along inherited structures, consistent with a distributed deformation field. The compressive
427 strain patch observed in the Eastern Carpathians (Fig. 6b) coincides with a cluster of thrust-faulting stress regime
428 indicators (Fig. 8), supporting the reliability of the GPS-derived strain inversion ~~derived from our estimated GPS~~
429 ~~velocities.~~ and illustrating how localized compression and extension coexist within the same regional stress
430 framework.

431 In the Moesian Platform, vertical movements are not uniform, but are accommodated differentially across crustal-
432 scale fault systems. This variability likely arises from the differing rheological properties of crustal blocks that
433 make up the MP (Mațenco et al., 2003; Petrescu et al., 2019) and the influence of pre-existing lithospheric
434 heterogeneities (e.g., Bertotti et al., 2003; Tărăpoancă et al., 2004). As a result, many fault mechanisms in the MP
435 exhibit both oblique and strike-slip components, producing seemingly chaotic fault patterns (Fig. 5). Focal
436 mechanism solutions in these regions may show greater variability, particularly in areas of pronounced strain
437 partitioning, such as near large-offset faults or shear zones.

438 6.3 Interactions between slab dynamics and surface uplift

439 Our results indicate a clear uplift trend in the foredeep basin area, supporting a typical post-collisional rebound
440 and uplift behavior, as observed in many other orogenic systems. These observations contrast with previous
441 models (van der Hoeven et al., 2005; Merten et al., 2005, 2010), which suggest that subsidence dominated the
442 evolution of the region as a typical response to slab subduction and retreat (Tărăpoancă et al., 2004). This is a key
443 ~~departure~~ ~~represents a notable change~~ from earlier interpretations, which ~~tended to highlight~~ ~~mainly focused on~~
444 uplift in the Dobrogea forebulge while assuming subsidence further towards the Carpathian Orogen. This is also
445 in line with some historical long-term repeated leveling methods (e.g., Popescu and Lazarescu, 1987; Joo, 1987)
446 and is further supported by recent InSAR analyses (Poncos et al., 2022). While the continued uplift in Dobrogea
447 is confirmed, the GPS data suggest that this uplift extends into the foredeep, highlighting the presence of vertical
448 motions in the foredeep basin that are not solely driven by active subduction dynamics.

449 The discrepancy may reflect either a shift in the tectonic regime over time or methodological limitations in
450 capturing ongoing geodynamic processes. The observed uplift may be associated with a partial decoupling
451 between the subducting lower lithosphere and the overlying crust (Petrescu et al., 2021), allowing stress relaxation
452 and isostatic rebound of the upper crust in the foreland. This scenario is consistent with the distribution of
453 intermediate-depth seismicity and the focal mechanism patterns observed in Vrancea. In addition, Mitrofan et al.
454 (2014) suggested a partial transmission of deformation from the slab to the crust, further supporting the idea of
455 vertical stress transfer from the mantle to the surface.

456 While the continued uplift in Dobrogea is confirmed, the GPS data suggest that this uplift extends into the
457 foredeep, highlighting the presence of vertical motions in the foredeep basin that are not solely driven by active

458 subduction dynamics. Instead, the observed uplift in both regions may be linked to slab break-off, a late-stage
459 process in the subduction and continental collision cycle (Andrews and Billen, 2009). As mentioned before, the
460 Dobrogea uplifting area at the transition to the Black Sea Basin is parallel with the SE Carpathians, suggesting
461 again the interplay between collisional processes affecting the Orogen and flexural response of the lower plate
462 with the forebulge outward (from the orogen) migration with coeval uplift and erosion.

463 Seismic imaging suggests that the Vrancea Sslab has partially torn and rotated at ~150 km depth (Martin et al.,
464 2006), leaving a deeper slab segment (200-310 km) still weakly attached (Heidbach et al., 2007). If break-off
465 continues to be active, asthenospheric upwelling through the torn slab segment (Petrescu et al., 2023) may be
466 dynamically supporting present-day uplift in both the SE Carpathians and foredeep. Numerical simulations of
467 subduction-collision systems with spontaneous slab break-off (Duretz et al., 2011) predict post-break-off uplift
468 rates of 0.1-0.8 km/Myr (0.1-0.8 mm/yr), which closely match our observed uplift. Additionally, an increase in
469 slab dip may promote low-wavelength lithospheric folding following continental collision (e.g., Cloetingh et al.,
470 2004; Mařenco et al., 2007), contributing further to the uplift observed in both the SE Carpathians and the
471 foredeep.

472 Our results also reveal a significant uplift in the East Carpathians (Fig. 4), not just the SE Carpathians, raising the
473 question of whether past slab break-off there (Nemcok et al. 1998) could still be influencing present-day vertical
474 motions. Geodynamic reconstructions suggest that the subducted passive margin of the East European Platform
475 progressively broke off from north to south along the East Carpathians (Sperner et al., 1996), culminating in the
476 currently detached Vrancea Sslab (Sperner et al., 2001; Koulakov et al., 2010; Lorincz and Houseman, 2010).
477 While the initial isostatic response to slab break-off is expected to occur within a few million years (Duretz et al.,
478 2011) or up to 7 million years after convergence stops (Andrews and Billen, 2009), prolonged effects such as
479 mantle flow, residual buoyancy, and lower-crustal flow could be sustaining regional uplift. This interpretation is
480 further supported by Bouguer gravity anomalies (Fig. 8), which show relatively positive values (0–40 mGal) over
481 the mountain belt, suggesting the presence of denser material at depth or incomplete isostatic compensation. The
482 north-to-south younging of post-collisional volcanism (Seghedi et al., 2004) suggests that slab detachment
483 propagated southward over time, with the East Carpathians experiencing earlier break-off than the SE Carpathians.
484 If asthenospheric upwelling and lithospheric weakening were significant during that time, they could have led to
485 prolonged crustal adjustments that continue to manifest as uplift today.

486 In addition to the SE and East Carpathians, we also identify localized uplift in the South Carpathians. This region
487 marks the collision between the Dacia Block and the Moesian Platform, where oblique thrusting over the thick
488 Moesian lithosphere (Mařenco et al., 1997) may be inducing flexural or isostatic responses (Bertotti et al., 2003).
489 Bouguer gravity anomalies in this area transition from strongly negative values (~-100 mGal) near the foredeep
490 in the south to over +100 mGal at the contact with the Transylvanian Basin (Fig. 8), indicating a shift from thick,
491 low-density crust to denser material in the north. This pattern suggests differential isostatic compensation, where
492 northward crustal thinning leads to less mass deficit and reduced buoyancy, potentially causing flexural uplift.
493 This contrast could drive vertical displacements, as observed. Alternatively, deeper mantle processes, such as
494 residual slab dynamics or lithospheric-scale deformation associated with orogenic curvature, may also influence
495 the observed uplift.

496 7. Conclusions

497 This study integrates the most stable and longest GPS data records over a period of 20 years in the Carpathian
498 region in Romania. Our results mark a significant improvement in spatial coverage and resolution of vertical and
499 horizontal crustal motions in a tectonically complex region sitting at the transition between dynamically active
500 subduction systems and the stable East European Platform, with additional influences exerted by a descending
501 slab.

502 We observe significant horizontal southward motion in the Moesian Platform, minimal motion in the
503 Transylvanian Basin and East Carpathians, and a slight north-west motion of the Eastern European Platform, in a
504 Eurasian reference frame. The relative motions between these regions generate ~~a complex strain rate pattern with~~
505 ~~zones of extension, compression, and shear, which closely align with observed regional seismic activity.~~ a
506 dominantly extensional strain field with localized zones of compression and shear, broadly consistent with stress
507 regimes inverted from earthquake clusters, although individual events capture more localized deformation
508 heterogeneity.

509 **Earlier studies in the region relied on campaign-style GPS observations. In contrast, our dataset includes cGPS**
510 **data from 130 stations spanning more than 20 years, providing improved spatial density and temporal resolution.**

511 Our extended and more reliable data also reveal uplift in the foredeep of the SE Carpathians, challenging a
512 previously held view that this area is solely subsiding based on temporary GPS station data. This insight provides
513 a fresh perspective on the region's slab dynamics, which may be influenced by slab break-off and the fragmented
514 nature of the foreland, with its blocks of varying rheological strength. These differential vertical motions are
515 accommodated by seismically active faults on a crustal scale.

516 Overall, this study significantly advances our understanding of the tectonic processes that shape regions at the
517 intersection of active subduction/collision zones and stable continental platforms. It provides fundamental
518 constraints on the interplay between slab dynamics, surface plate kinematics, and the resulting crustal
519 deformation, an essential step toward improving seismic hazard assessment.

520 Code availability

521 The GipsyX software is licensed to the Department of Geophysics of the University of Bucharest (UNIBUC). We
522 were allowed to use this software in an ongoing collaboration with UNIBUC. Strain rate estimation codes are
523 freely available at <https://github.com/DSOlab/StrainTool> (accessed in January 2025). Most figures were made
524 using the open-source GMT software (Wessel et al., 2013).

525 Data availability

526 ~~The data that support the findings of this study are available from the corresponding author upon reasonable~~
527 ~~request.~~ **The RINEX-format GNSS data (sampled at 30s intervals) analysed in this study are only available from**
528 **the NIEP (National Institute of Earth Physics) network online at <http://gps.infp.ro/#/>.** The rest of the data can be
529 **made available from the organisations responsible with their maintenance upon reasonable request and data**

530 sharing agreements. All individual velocity solutions and strain rate estimates from this study are provided in the
531 Supplementary Material.

532 **Author contributions**

533 **AM:** Conceptualization, Methodology, Data Curation, Formal analysis, Investigation, Writing - Original Draft,
534 Visualization **LP:** Formal analysis, Writing - Original Draft, Visualization **BA:** Software, Data Curation, Formal
535 analysis, Visualization, Writing - Review & Editing, Supervision **FB:** Writing - Review & Editing **EN:** Writing -
536 Review & Editing, Installation and Stations Maintenance **IM:** Writing - Review & Editing

537 **Competing interests**

538 The authors declare that they have no conflict of interest.

539 **Acknowledgments**

540 ~~We gratefully acknowledge Prof. Dr. V. Mocanu, who, in 2001, initiated the establishment of the first seven~~
541 ~~dedicated continuous GPS (cGPS) stations in Romania, together with our esteemed late colleague L. Munteanu~~
542 ~~and a consortium of Dutch universities. Their early efforts laid the groundwork for long term geodetic and~~
543 ~~geophysical research in the region.~~

544 **We acknowledge the Netherlands Research Centre for Integrated Solid Earth Science (ISES) for the initial**
545 **establishment in 2001 of seven cGPS stations in Romania dedicated to long term geodetic and geophysical**
546 **research in the region. This early enterprise comprised a collaborative effort of the University of Bucharest (V.**
547 **Mocanu), the National Institute for Earth Physics (L. Munteanu), the Delft University of Technology (B.A.C.**
548 **Ambrosius) and the Utrecht University (W. Spakman).** We thank the National Research and Development Institute
549 for Marine Geology and Geo-Ecology, National Center for Monitoring and Alarm to Natural Marine Hazards –
550 Euxinus, as well as the National Agency for Cadaster and Land Registration, and the TopGeocart company for
551 providing access to their data.

552 **Financial support**

553 This research was carried out within the NUCLEU project, SOL4RISC Program which is supported by the
554 Ministry of Education and Research, project nr. PN23360201. This work was also supported by the European
555 Union (Next Generation EU instrument) through the National Recovery and Resilience Plan, "PNRR-III-C9-2022
556 – I5 Establishment and operationalization of Competence Centers" competition, "Competence Center for Climate
557 Change Digital Twin for Earth forecasts and societal redressment: DTEClimate" project, contract
558 no.760008/30.12.2022, code 7/16.11.2022.

559

560

561

562 **References**

- 563 ~~Altamimi, Z., Rebischung, P., Métivier, L., Collilieux, X.: ITRF2014: a new release of the International Terrestrial~~
564 ~~Reference Frame modeling nonlinear station motions, *J. Geophys. Res. Sol. Ea.*, 121, 6109–6131,~~
565 ~~<https://doi.org/10.1002/2016JB013098>, 2016.~~
- 566 **Altamimi, Z., Métivier, L., Rebischung, P., Rouby, H., and Collilieux, X.: ITRF2014 plate motion model,**
567 ***Geophys. J. Int.*, 209, 1906–1912, <https://doi.org/10.1093/gji/ggx136>, 2017.**
- 568 **Anastasiou D.G., Papanikolaou X., Ganas A., and Paradissis D.: StrainTool: A software package to estimate strain**
569 **tensor parameters. *Zenodo*; Version 1.1, <https://doi.org/10.5281/zenodo.5501234>, 2021.**
- 570 Amaru, M. L.: Global travel time tomography with 3-D reference models, PhD thesis, Utrecht Univ., Utrecht,
571 Netherlands, 2007.
- 572 Andrews, E. R. and Billen, M. I.: Rheologic controls on the dynamics of slab detachment, *Tectonophysics*, 464,
573 60-69, <https://doi.org/10.1016/j.tecto.2007.09.004>, 2009.
- 574 ~~Armeanu, I., Chircea, A., Ciobanu, I., Craiu, A., Craiu, G. M., Dinescu, R., Mihai, M., Predoiu, A., Tolea,~~
575 ~~A., Varzaru, L. C., Borleanu, F., Neagoe, C., Radulian, M., and Mihaela, P.: Database of the 2023 seismic~~
576 ~~sequence recorded in Gorj area (Romania), *Mendeley Data*, V1, <https://doi.org/10.17632/ds4hwchkp7.1>, 2023.~~
- 577 Bada, G., Horváth, F., Dövényi, P., Szafián, P., Windhoffer, G. and Cloetingh, S.: Present-day stress field and
578 tectonic inversion in the Pannonian basin, *Global Planet. Change*, 58, 165-180,
579 <https://doi.org/10.1016/j.gloplacha.2007.01.007>, 2007.
- 580 Balla, Z.: Palaeotectonic reconstruction of the central Alpine-Mediterranean belt for the Neogene,
581 *Tectonophysics*, 127, 213-243, [https://doi.org/10.1016/0040-1951\(86\)90062-4](https://doi.org/10.1016/0040-1951(86)90062-4), 1986.
- 582 Bertiger, W., Bar-Sever, Y., Dorsey, A., Haines, B., Harvey, N., Hemberger, D., Heflin, M., Lu, W., Miller, M.,
583 Moore, A.W., Murphy, D., Ries, P., Romans, L., Sibois, A., Sibthorpe, A., Szilagy, B., Vallisneri, M., and Willis,
584 P.: GipsyX/RTGx, a new tool set for space geodetic operations and research, *Advances in Space Research*, 66,
585 469–489, <https://doi.org/10.1016/j.asr.2020.04.015>, 2020.
- 586 Bertotti, G., Maţenco, L. and Cloetingh, S. A. P. L.: Vertical movements in and around the south-east Carpathian
587 foredeep: lithospheric memory and stress field control. *Terra Nova*, 15, 299-305, 2003.
- 588 Beşuţiu, L., Manca, V., Pomeran, M.: Vrancea seismic zone as an unstable triple junction: new evidence from
589 observations and numerical modelling. In: 9th Congress of the Balkan Geophys. Soc, vol. 2017. European
590 Association of Geoscientists & Engineers, 1-5, 2017 <https://doi.org/10.3997/2214-4609.201702541>
- 591 Blewitt, G., Lavallée, D., Clarke, P., and Nurutdinov, K.: A new global mode of Earth deformation: Seasonal
592 cycle detected, *Science*, 294, 2.342-2.345, <https://doi.org/10.1126/science.106532001>, 2001.
- 593 Bonvalot, S., Balmino, G., Briais, A., M. Kuhn, Peyrefitte, A., Vales, Biancale, R., Gabalda, G., Moreaux, G.,
594 Reinquin, F., and Sarrailh, M.: World Gravity Map, 1:50000000 map, Eds.: BGI-CGMW-CNES-IRD, Paris, 2012.
- 595 Bos. M. S., and Scherneck, H., G.: ~~Chalmers University of Technology~~, Ocean tide loading provider,
596 <http://holt.oso.chalmers.se/loading/index.html>, 2011.
- 597 Borleanu F., Petrescu L., Fojtikova L., Munteanu I., Silvennoinen H., Placinta A.O., Oros E., and Enescu B.: ML
598 5.7 Southern Carpathians earthquake sequence: Insights from seismic observations, ESC2024-S17/50-808,
599 https://www.erasmus.gr/UsersFiles/microsite1277/Documents/ESC2024_Abstract_Book.pdf, 2024.
- 600 Cloetingh, S. A. P. L., Burov, E., Matenco, L., Toussaint, G., Bertotti, G., Andriessen, P. A. M., Wortel, M. J. R.
601 and Spakman, W.: Thermo-mechanical controls on the mode of continental collision in the SE Carpathians
602 (Romania), *Earth Planet. Sc. Lett.*, 218, 57-76, 2004.
- 603 Cloetingh, S., Bada, G., Maţenco, L., Lankreijer, A., Horváth, F. and Dinu, C.: Modes of basin (de) formation,
604 lithospheric strength and vertical motions in the Pannonian-Carpathian system: inferences from thermo-
605 mechanical modelling, *Geo. Soc. Mem.*, 32, 207-221, DOI: 10.1144/GSL.MEM.2006.032.01.12, 2006.
- 606 Cornea, I., Dragoescu, I., Popescu, M. N., and Visarion, M.: Monography of recent vertical crustal movements in
607 the S. R. of Romania (in Romanian), Preprint Central Inst. of Phys., 100, 1978.

- 608 Cornea, I., and Popescu, M. N.: The Vrancea Earthquake of March 4. 1977 and the Recent crustal vertical
609 movements in Romania. In Cornea & Radu (Editors): Seismological Research of March 4. 1977 Earthquake (in
610 Romanian), Preprint Central Inst. of Phys., 559 - 568, 1979a.
- 611 Cornea, I., Dragoescu, I., Popescu, M. N., and Visarion, M.: Map of recent vertical crustal movements of the
612 territory of S. R. of Romania (in Romanian), St. Cerc. Geol., Geofiz., Geogr., Geofizica, 17, 3-20, 1979b.
- 613 Craiu, A., Craiu, M., Diaconescu, M. and Marmureanu, A.: 2013 Seismic swarm recorded in Galati area,
614 Romania: focal mechanism solutions, Acta Geod. Geophys., 52, 53-67, 2017.
- 615 Csontos, L., and Vörös, A.: Mesozoic plate tectonic reconstruction of the Carpathian region, Palaeogeography,
616 Palaeoclimatology, Palaeoecology, 210, 1-56, <https://doi.org/10.1016/j.palaeo.2004.02.033>, 2004.
- 617 Dinter, G., and Schmitt, G.: Three Dimensional Plate Kinematics in Romania, Nat. Hazards, 23, 389-406,
618 <https://doi.org/10.1023/A:1011116615142>, 2001.
- 619 Duretz, T., Gerya, T. V. and May, D. A.: Numerical modelling of spontaneous slab breakoff and subsequent
620 topographic response, Tectonophysics, 502, 244-256, <https://doi.org/10.1016/j.tecto.2010.05.024>, 2011.
- 621 **Enescu, B., Ghita, C., Moldovan, I.A. and Radulian, M.: Revisiting Vrancea (Romania) intermediate-depth**
622 **seismicity: some statistical characteristics and seismic quiescence testing. Geosciences, 13, 21,**
623 **<https://doi.org/10.3390/geosciences13070219>, 2023.**
- 624 Heidbach, O., Ledermann, P., Kurfeß, D., Peters, G., Buchmann, T., Matenco, L., Negut, M., Sperner, B., Müller,
625 B., and Nuckelt, A.: Attached or not attached: slab dynamics beneath Vrancea, Romania, In: International
626 symposium on strong Vrancea earthquakes and risk mitigation, 4-20, 2007.
- 627 Heidbach, O., Rajabi, M., Cui, X., Fuchs, K., Müller, B., Reinecker, J., Reiter, K., Tingay, M., Wenzel, F., Xie,
628 F. and Ziegler, M.O.: The World Stress Map database release 2016: Crustal stress pattern across scales.
629 Tectonophysics, 744, 484-498, 2018
- 630 Hippolyte, J.C.: Geodynamics of Dobrogea (Romania): new constraints on the evolution of the Tornquist-
631 Teisseyre Line, the Black Sea and the Carpathians, Tectonophysics, 357, 33-53, [https://doi.org/10.1016/S0040-1951\(02\)00361-X](https://doi.org/10.1016/S0040-1951(02)00361-X), 2002.
- 633 ~~Ionescu, C., and Neagoe, C.: Romanian seismic network development, Acta Geod. Geophys. Hu., 43, 145-152~~
634 ~~DOI: 10.1556/AGeod.43.2008.2-3.4, 2008.~~
- 635 Ismail-Zadeh, A., Mañenco, L., Radulian, M., Cloetingh, S. and Panza, G.: Geodynamics and intermediate-depth
636 seismicity in Vrancea (the south-eastern Carpathians): current state-of-the art. Tectonophysics, 530, 50-79, DOI:
637 10.1016/j.tecto.2012.01.016, 2012.
- 638 Joó, I., Arabadžijski, D., Fűry, M., Meščerski, I. N., Mihăila, M., Mladenovski, M. M., Németh, Z., Steinberg, J.,
639 Thury, J., Vanko, J., and Wyrzykowski, T.: New investigations on recent vertical movements in the Carpatho-
640 Balkan region, J. Geodyn., 8, 99-113, [https://doi.org/10.1016/0264-3707\(87\)90028-7](https://doi.org/10.1016/0264-3707(87)90028-7), 1987.
- 641 Koulakov, I., Zaharia, B., Enescu, B., Radulian, M., Popa, M., Parolai, S. and Zschau, J.: Delamination or slab
642 detachment beneath Vrancea? New arguments from local earthquake tomography, Geochem. Geophys. Geosy.,
643 11, <https://doi.org/10.1029/2009GC002811>, 2010.
- 644 Krézsek, C., Lăpădat, A., Mañenco, L., Arnberger, K., Barbu, V., and Olaru, R.: Strain partitioning at orogenic
645 contacts during rotation, strike-slip and oblique convergence: Paleogene-Early Miocene evolution of the contact
646 between the South Carpathians and Moesia, Global Planet. Change, 103, 63-81, <https://doi.org/10.1016/j.gloplacha.2012.11.009>, 2013.
- 648 Lorinczi, P., and Houseman, G.: Lithospheric gravitational instability beneath the Southeast Carpathians,
649 Tectonophysics, 474, 322-336, <https://doi.org/10.1016/j.tecto.2008.05.024>, 2009.

- 650 Mațenco L, Zoetemeijer R, Cloetingh S, and Dinu C.: Lateral variations in mechanical properties of the Romanian
651 external Carpathians: inferences of flexure and gravity modelling. *Tectonophysics*, 282,147-166, 1997.
- 652 Mațenco, L., and Bertotti, G.: Tertiary tectonic evolution of the external East Carpathians (Romania),
653 *Tectonophysics*, 316, 255–286, [https://doi.org/10.1016/S0040-1951\(99\)00261-9](https://doi.org/10.1016/S0040-1951(99)00261-9), 2000.
- 654 Mațenco L, Bertotti G, Cloetingh S, and Dinu C; Subsidence analysis and tectonic evolution of the external
655 Carpathian-Moesian platform region during Neogene times. *Sed Geol*, 156(14), 71-94, 2003.
- 656 Mațenco, L., Bertotti, G., Leever, K., Cloetingh, S.A.P.L., Schmid, S.M., Tărăpoancă, M., and Dinu, C.: Large-
657 scale deformation in a locked collisional boundary: Interplay between subsidence and uplift, intraplate stress, and
658 inherited lithospheric structure in the late stage of the SE Carpathians evolution, *Tectonics*, 26,
659 <https://doi.org/10.1029/2006TC001951>, 2007.
- 660 Merten, S., Andriessen, P. A. M., Juez-Larré, J., Bertotti, G. V., and Dunai, T. J.: Dating the exhumation of the
661 Romanian Carpathians: first results from apatite (U-Th)/He thermochronology, *Abstract from Geophysical
662 Research Abstracts*, 7, 08138, <https://meetings.copernicus.org/www.cosis.net/abstracts/EGU05/08138/EGU05-J-08138.pdf>, 2005.
- 664 Merten S., Matenco L., Foeken J. P. T., Stuart F. M., and Andriessen P. A. M.: From nappe stacking to out-of-
665 sequence postcollisional deformations: Cretaceous to Quaternary exhumation history of the SE Carpathians
666 assessed by low-temperature thermochronology, *Tectonics*, 29, <https://doi.org/10.1029/2009TC002550>, 2010.
- 667 Mrazec L., and Voitești I.P.: Contribuții la cunoașterea panzelor flisului carpatic (in Romanian), *An. Inst. Geol.
668 Rom.*, V, 495-521, 1914.—
- 669 Müller, B., Heidbach, O., Negut, M., Sperner, B. and Buchmann, T.: Attached or not attached—evidence from
670 crustal stress observations for a weak coupling of the Vrancea slab in Romania, *Tectonophysics*, 482, 139-149,
671 <https://doi.org/10.1016/j.tecto.2009.08.022>, 2010.
- 672 Necea, D., Fielitz, W., and Matenco, L.: Late Pliocene–Quaternary tectonics in the frontal part of the SE
673 Carpathians: Insights from tectonic geomorphology, *Tectonophysics*, 410, 137-156,
674 <https://doi.org/10.1016/j.tecto.2005.05.047>, 2005.
- 675 Necea D., Fielitz W., Kadereit A., P.A.M. Andriessen P.A.M., and Dinu C.: Middle Pleistocene to Holocene
676 fluvial terrace development and uplift-driven valley incision in the SE Carpathians, Romania, *Tectonophysics*,
677 602, 332-354, <https://doi.org/10.1016/j.tecto.2013.02.039>, 2013.
- 678 Necea, D., Juez-Larré, J., Matenco, L., Andriessen, P. A.M., and Dinu C.: Foreland migration of orogenic
679 exhumation during nappe stacking: Inferences from a high-resolution thermochronological profile over the
680 Southeast Carpathians, *Global Planet. Change*, 200, 103457, <https://doi.org/10.1016/j.gloplacha.2021.103457>,
681 2021.
- 682 Nemcok, M., Pospisil, L., Lexa, J., and Donelick, R.A.: Tertiary subduction and slab break-off model of the
683 Carpathian–Pannonian region, *Tectonophysics*, 295, 307-340, [https://doi.org/10.1016/S0040-1951\(98\)00092-4](https://doi.org/10.1016/S0040-1951(98)00092-4),
684 1998.
- 685 Petrescu, L., Stuart, G., Tataru, D., and Grecu, B.: Crustal structure of the Carpathian Orogen in Romania from
686 receiver functions and ambient noise tomography: how craton collision, subduction and detachment affect the
687 crust. *Geophys. J. Int.*, 218, 163-178, <https://doi.org/10.1093/gji/ggz140>, 2019.
- 688 Petrescu, L., Borleanu, F., Radulian, M., Ismail-Zadeh, A., and Mațenco, L.: Tectonic regimes and stress patterns
689 in the Vrancea Seismic Zone: Insights into intermediate-depth earthquake nests in locked collisional settings,
690 *Tectonophysics*, 799, 228688, <https://doi.org/10.1016/j.tecto.2020.228688>, 2021.
- 691 Petrescu, L., Mihai, A. and Borleanu, F.: Slab tear and rotation imaged with core-refracted shear wave anisotropy.,
692 *J. Geodyn.*, 157, 101985, <https://doi.org/10.1016/j.jog.2023.101985>, 2023.
- 693 Petrescu, L. and Enescu, B.: Seismicity of a relic slab: space–time cluster analysis in the Vrancea Seismic Zone.
694 *Earth, Planets and Space*, 77, 6, <https://doi.org/10.1186/s40623-025-02136-6>, 2025.
- 695 Piña-Valdés, J., Socquet, A., Beauval, C., Doin, M.-P., D’Agostino, N., and Shen, Z.-K.: 3D GNSS velocity field
696 sheds light on the deformation mechanisms in Europe: Effects of the vertical crustal motion on the distribution of
697 seismicity, *J. Geophys. Res.-Sol. Ea.*, 127, e2021JB023451, <https://doi.org/10.1029/2021JB023451>, 2022.

- 698 Poncos, V., Stanciu, I., Teleaga, D., Maţenco, L., Bozsó, I., Szakács, A., Birtas, D., Toma, S.A., Stanica, A., and
699 Radulescu, V.: An Integrated Platform for Ground-Motion Mapping, Local to Regional Scale; Examples from SE
700 Europe. *Remote Sensing*, 14, 1046, [10.3390/rs14041046](https://doi.org/10.3390/rs14041046), 2022.
- 701 Popa, M., Chircea, A., Dinescu, R., Neagoe, C., Grecu, B., and Borleanu, F.: Romanian earthquake catalogue
702 (ROMPLUS). *Mendeley Data*, 2, 2022.
- 703 Popescu, M. N., and Drăgoescu, I.: Maps of recent vertical crustal movements in Romania: Similarities and
704 differences, *J. Geodyn.*, 8, 123-136, [https://doi.org/10.1016/0264-3707\(87\)90030-5](https://doi.org/10.1016/0264-3707(87)90030-5), 1987.
- 705 ~~Radulescu F.: Romanian seismology—historical, scientific and human landmarks *Rev. Roum. Geophysique*, 52–
706 53, 101–121, 2008–2009.~~
- 707 Radulian, M., Bălă, A., Ardeleanu, L., Toma-Dănilă, D., Petrescu, L., and Popescu, E.: Revised catalogue of
708 earthquake mechanisms for the events occurred in Romania until the end of twentieth century: REFMC, *Acta
709 Geod. Geophys.*, 54, 3-18, <https://doi.org/10.1007/s40328-018-0243-y>, 2019.
- 710 Radulian, M., Popa, M., Dinescu, R., and Bala, A.: Location improvements for the twin crustal earthquakes
711 recorded in February 2023 in Gorj County, Romania. *International Multidisciplinary Scientific GeoConference:
712 SGEM*, 23(1.1), 57-64, 2023.
- 713 Ren, Y., Stuart, G., Houseman, G., Dando, B., Ionescu, C., Hegedüs, E., Radovanović, S., and Shen, Y.: Upper
714 mantle structures beneath the Carpathian–Pannonian region: Implications for the geodynamics of continental
715 collision, *Earth Planet. Sc. Lett.*, 349, 139–152. <https://doi.org/10.1016/j.epsl.2012.06.037>, 2012.
- 716 re3data.org: VMF Data Server; editing status 2024-05-15; re3data.org - Registry of Research Data Repositories,
717 <https://doi.org/10.17616/R3RD2H>
- 718 Sanders, C., Andriessen, P., and Cloetingh, S.: Life cycle of the East Carpathian orogen: erosion history of a
719 doubly vergent critical wedge assessed by fission track thermochronology, *J. Geophys. Res.*, 104, 29095–29112,
720 <https://doi.org/10.1029/1998JB900046>, 1999.
- 721 Schmid, S.M., Fügenschuh, B., Kounov, A., Maţenco, L., Nievergelt, P., Oberhänsli, R., Pleuger, J., Schefer, S.,
722 Schuster, R., Tomljenović, B., and Ustaszewski, K.: Tectonic units of the Alpine collision zone between Eastern
723 Alps and western Turkey, *Gondwana Res.*, 78, 308-374, <https://doi.org/10.1016/j.gr.2019.07.005>, 2020.
- 724 Seghedi, A., Lang, B. and Heimann, A.: The deformational history of North Dobrogean Hercynian basement as
725 reflected in new ³⁹Ar/⁴⁰Ar determinations, *Romanian Journal of Tectonics and Regional Geology*, 77, 64-62,
726 <https://doi.org/10.3906/YER-1101-20>, 1999.
- 727 Seghedi, I., Downes, H., Vaselli, O., Szakács, A., Balogh, K. and Pécskay, Z.: Post-collisional Tertiary–
728 Quaternary mafic alkalic magmatism in the Carpathian–Pannonian region: a review, *Tectonophysics*, 393, 43-62,
729 <https://doi.org/10.1016/j.tecto.2004.07.051>, 2004.
- 730 Serpelloni, E., Cavaliere, A., Martelli, L., Pintori, F., Anderlini, L., Borghi, A., Randazzo, D., Bruni, S., Devoti,
731 R., Perfetti, P., and Cacciaguerra, S.: Surface Velocities and Strain-Rates in the Euro-Mediterranean Region From
732 Massive GPS Data Processing, *Front. Earth Sci.*, 10, 907897, <https://doi.org/10.3389/feart.2022.907897>, 2022.
- 733 Shen, Z. K., Wang, M., Zeng, Y., and Wang, F.: Strain determination using spatially discrete geodetic data, *Bull.
734 Seismol. Soc. Am.*, 105, 2117-2127, <https://doi.org/10.1785/0120140247>, 2015.
- 735 Sperner, B.: Computer programs for the kinematic analysis of brittle deformation structures and the Tertiary
736 tectonic evolution of the Western Carpathians. *Tübingen Geoscientific Works (TGA) Series A. Geology,
737 Paleontology, Stratigraphy* 27 (NEBIS)001536648EBI01, 1996.
- 738 Sperner, B., Lorenz, F., Bonjer, K., Hettel, S., Müller, B., and Wenzel, F: Slab break-off–abrupt cut or gradual
739 detachment? New insights from the Vrancea Region (SE Carpathians, Romania), *Terra Nova*, 13, 172-179,
740 <https://doi.org/10.1046/j.1365-3121.2001.00335.x>, 2001.
- 741 Tărăpoancă, M., Garcia-Castellanos, D., Bertotti, G., Matenco, L., Cloetingh, S., and Dinu, C.: Role of the 3-D
742 distributions of load and lithospheric strength in orogenic arcs: polystage subsidence in the Carpathians foredeep,
743 *Earth Planet. Sc. Lett.*, 221, 163–180, [https://doi.org/10.1016/S0012-821X\(04\)00068-8](https://doi.org/10.1016/S0012-821X(04)00068-8), 2004.

- 744 Van der Hoeven, A., Mocanu, V., Spakman, W., Nutto, M., Nuckelt, A., Matenco, L., Munteanu, L., Marcu, C.,
745 and Ambrosius, B.: Observation of present-day tectonic motions in the Southeastern Carpathians: Results of the
746 ISES/CRC-461 GPS measurements, *Earth Planet. Sc. Lett.*, 239, 177-
747 184, <https://doi.org/10.1016/j.epsl.2005.09.018>, 2005.
- 748 Wenzel, F., Lorenz, F., Sperner, B., and Oncescu, M. C.: Seismotectonics of the Romanian Vrancea area, Vrancea
749 Earthquakes: Tectonics, Hazard and Risk Mitigation, 15–26, Kluwer Acad., 1999.
- 750 Wessel, P., W. H. Smith, R. Scharroo, J. Luis, and F. Wobbe: Generic Mapping Tools: Improved Version
751 Released, *Eos, Trans. AGU*, 94 (45), 409–410, <https://doi.org/10.1002/2013EO450001>, 2013.
- 752 Wortel, M.J.R. and Spakman, W.: Subduction and slab detachment in the Mediterranean-Carpathian region,
753 *Science*, 290, 1910-1917, <https://doi.org/10.1126/science.290.5498.1910>, 2000.